



HAL
open science

Two novel COLVI long chains in zebrafish that are essential for muscle development

Laetitia Ramanoudjame, Claire Rocancourt, Jeanne Lainé, Arnaud Klein, Lucette Joassard, Corine Gartioux, Marjory Fleury, Laura Lyphout, Edor Kabashi, Sorana Ciura, et al.

► **To cite this version:**

Laetitia Ramanoudjame, Claire Rocancourt, Jeanne Lainé, Arnaud Klein, Lucette Joassard, et al.. Two novel COLVI long chains in zebrafish that are essential for muscle development. *Human Molecular Genetics*, 2015, 24 (23), pp.6624-6639. 10.1093/hmg/ddv368 . hal-01594462

HAL Id: hal-01594462

<https://hal.science/hal-01594462v1>

Submitted on 11 Nov 2024

HAL is a multi-disciplinary open access archive for the deposit and dissemination of scientific research documents, whether they are published or not. The documents may come from teaching and research institutions in France or abroad, or from public or private research centers.

L'archive ouverte pluridisciplinaire **HAL**, est destinée au dépôt et à la diffusion de documents scientifiques de niveau recherche, publiés ou non, émanant des établissements d'enseignement et de recherche français ou étrangers, des laboratoires publics ou privés.

Two novel COLVI long chains in zebrafish that are essential for muscle development

Ramanoudjame Laetitia^{1,2}, Rocancourt Claire³, Lainé Jeanne^{1,2,4}, Klein Arnaud^{1,2}, Joassard Lucette³, Gartioux Corine^{1,2}, Fleury Marjory^{1,2}, Lyphout Laura³, Kabashi Edor⁵, Ciura Sorana⁵, Cousin Xavier^{3,6}, Allamand Valérie^{1,2,*}

¹ Univ Paris 06, Univ Paris 04, Ctr Rech Myol,UMRS974, INSERM,CNRS FRE3617, F-75651 Paris 13, France.

² Inst Myol, F-75013 Paris, France.

³ IFREMER, Fish Ecophysiol Grp, F-17137 Lhoumeau, France.

⁴ Univ Paris 06, Univ Paris 04, Dept Physiol, F-75013 Paris, France.

⁵ Univ Paris 06, Univ Paris 04,INSERM U 1127, CNRS UMR 1127, Inst Cerveau & Moelle Epiniere ICM,UMR 7225, Paris, France.

⁶ INRA LPGP, F-35042 Rennes, France.

* Corresponding author / Valérie Allamand, email address : v.allamand@institut-myologie.org

Abstract :

Collagen VI (COLVI), a protein ubiquitously expressed in connective tissues, is crucial for structural integrity, cellular adhesion, migration and survival. Six different genes are recognized in mammals, encoding six COLVI-chains that assemble as two 'short' ($\alpha 1$, $\alpha 2$) and one 'long' chain (theoretically any one of $\alpha 3-6$). In humans, defects in the most widely expressed heterotrimer ($\alpha 123$), due to mutations in the *COL6A1-3* genes, cause a heterogeneous group of neuromuscular disorders, collectively termed COLVI-related muscle disorders. Little is known about the function(s) of the recently described $\alpha 4-6$ chains and no mutations have been detected yet. In this study, we characterized two novel COLVI long chains in zebrafish that are most homologous to the mammalian $\alpha 4$ chain; therefore, we named the corresponding genes *col6a4a* and *col6a4b*. These orthologues represent ancestors of the mammalian *Col6a4-6* genes. By *in situ* hybridization and RT-qPCR, we unveiled a distinctive expression kinetics for *col6a4b*, compared with the other *col6a* genes. Using morpholino antisense oligonucleotides targeting *col6a4a*, *col6a4b* and *col6a2*, we modelled partial and complete COLVI deficiency, respectively. All morphant embryos presented altered muscle structure and impaired motility. While apoptosis was not drastically increased, autophagy induction was defective in all morphants. Furthermore, motoneuron axon growth was abnormal in these morphants. Importantly, some phenotypical differences emerged between *col6a4a* and *col6a4b* morphants, suggesting only partial functional redundancy. Overall, our results further confirm the importance of COLVI in zebrafish muscle development and may provide important clues for potential human phenotypes associated with deficiency of the recently described COLVI-chains.

Introduction

Collagens are major components of extracellular matrices (ECM) (1), complex structures that ensure tissue architecture and play diverse biological functions. Collagen VI (COLVI), a unique member of this large family, is ubiquitously expressed and has been involved in tissue integrity, cell survival and signalling (2-10). To date, 6 different genes are recognized in mammals, encoding 6 different α chains (11). COLVI assembly is a complex, multi-step process that begins with the formation of monomers composed of 2 short (invariably $\alpha 1$ and $\alpha 2$) and one long chain that may vary (either one of $\alpha 3-6$) (12-14). These monomers further form dimers and tetramers that are secreted into the ECM where they align into beaded microfibrils (15-19).

While the most widespread and best characterized COLVI heterotrimer contains the $\alpha 1$, $\alpha 2$ and $\alpha 3$ chains, the $\alpha 4-6$ long chains have been described more recently in human and mouse (14, 20). In vertebrates, orthologs of the corresponding genes are organized in tandem at the same locus (5' *Col6a4*, *Col6a5*, *Col6a6* 3'), with the exception of human, gorilla and chimpanzee where the *COL6A4* gene is only partial due to a pericentric inversion that occurred before the branching of hominoids (11). The two halves of the human *COL6A4* gene, located on both arms of chromosome 3, were initially considered as pseudogenes; nevertheless, the 5' part of the split *COL6A4* gene on chromosome 3p24.3 has been associated with osteoarthritis as the *DVWA* gene, and appears to be expressed intracellularly (21, 22).

Similarly to the $\alpha 3$ chain, the $\alpha 4-6$ mature proteins are composed of seven N-terminal von Willebrand factor A-like (vWFA) domains (N7–N1), followed by a 336-amino acid-long collagen triple helical domain (THD) classically containing [Gly-X-Y] triplets. They display two consecutive vWFA domains (C1 and C2) as well as unique sequences (C3) toward the C-terminus. In addition, the murine $\alpha 4$ chain carries 17 amino acid residues at its C-terminal end that constitute a partial Kunitz protease inhibitor domain. The C-terminus of $\alpha 5$ further

extends with the presence of a third vWFA domain (C4) and a second unique stretch of 130 amino acids (C5) (reviewed in (11)).

The murine *Col6a4-6* genes are positioned on chromosome 9. Their expressions differ in their spatial pattern, and are developmentally regulated (14, 20). Importantly, $\alpha 4$ is not expressed in adult murine skeletal muscle, but both $\alpha 5$ and $\alpha 6$ are, only partially co-localizing with $\alpha 3$.

Mutations in either of the *COL6A1*, *COL6A2* or *COL6A3* gene lead to COLVI-related muscle disorders, a heterogeneous group of clinical presentations ranging from Ullrich Congenital Muscular Dystrophy (UCMD; MIM#254090; (23)) to Bethlem Myopathy (BM; MIM#158810; (24)), with intermediate phenotypes. The most prominent symptoms caused by COLVI deficiency affect skeletal muscle, joints, as well as skin (reviewed in (25-27)). Interestingly, patients with COLVI-related myopathies have altered expressions of $\alpha 5$ and $\alpha 6$ in skin and skeletal muscle (28-30). However, to date, there are no reported mutations in the *COL6A5-6* genes, and their involvement in human disease(s) remains unknown.

Over the last 15 years or so, zebrafish (*Danio rerio*) has become increasingly used as a model for neuromuscular disorders (31, 32). Its rapid development enables easy analysis of motility defects as early as 2 days post fertilization (dpf). More than 80% of the genes implicated in human muscle diseases have zebrafish orthologs, and muscle structure organization between the 2 species is similar (33). Somites are separated by vertical myosepta, equivalent to tendons, to which myofibres attach through myotendinous junctions (34). Slow muscle cells form a superficial monolayer in embryos and later remain at the periphery of the myotome, while fast muscle cells are located deep within the myotome, making up most of the trunk musculature (35).

Here we report and characterize the orthologs, and we believe ancestors, of mammalian *Col6a4-6* in the zebrafish genome. We examined their temporal and spatial

expression at different developmental stages. We further showed that their knock-down leads to muscle defects, reminiscent of those observed in *col6a2* deficiency, although some specific features emerged. We thus confirm the importance of the *col6* genes in zebrafish muscle development and provide new insights on the potential roles of the recently described α 4-6 chains.

Results

Identification of two novel col6 genes in zebrafish

To identify zebrafish orthologs of the mammalian α 4-6 chains (reviewed in (11)), the protein sequences of human α 5-6 (NP_001265227.1 and NP_001096078.1, respectively) and mouse α 4-6 (NP_081039.2, NP_001161395.1 and NP_001096077.1, respectively) were used in a BLAST search against the zebrafish genome at ENSEMBL. Two novel proteins were identified. Since their C-terminus domains were similar in size and organisation, these parts of the proteins were aligned to other vertebrate Col6 proteins and a phylogenetic tree was inferred using the ClustalX software, revealing that the zebrafish proteins are phylogenetically closer to Col6a4 than to either Col6a5 or Col6a6, or even Col6a3 (Fig. 1A, Fig. S1 and S2). The corresponding genes, located on chromosomes 16 and 13, were thus named *col6a4a* and *col6a4b*, respectively (Fig. 1B). These genes likely represent ancestors of the mammalian Col6a4-6 genes. The zebrafish α 4a (2568 amino acids) and α 4b (2497 amino acids) chains present common features of all COLVI peptides, such as the conserved triple helical domain containing [Gly-X-Y] repeats (336 and 303 amino acids long for α 4a and α 4b, respectively), flanked by large globular domains with homologies to vWFA domains (8 and 2 in N- and C-terminal, respectively). In addition, they also possess 2 Kunitz domains in C-terminal, which are only present in mammalian α 3 and α 4 chains (Fig. 1B). In contrast, no fibronectin III domain was found in C-terminal, contrary to α 3 (Fig. S1). Multiple sequence alignments between human, mouse and zebrafish α 3-6 proteins are presented in Fig. S2.

Knockdown of col6a genes in zebrafish embryos

To further understand the function of the *col6a4a* and *col6a4b* gene products, we designed acceptor splice site morpholinos (MOs) targeting *col6a4a* exon11 (MO-a4a) and *col6a4b* exon 12 (MO-a4b) (Fig. 1B). The resulting splicing events induce frameshifts that create premature termination codons (PTC). We also used this strategy to knockdown *col6a2* expression with a MO against exon 2 (MO-a2; Fig. 1C), to obtain reference morphants deficient in this crucial short chain present in all heterotrimers. A mismatch morpholino (scramble) with no biological target was injected as a control of specificity.

Knockdown efficacy was assessed by Northern blotting using total RNA extracted from 48hpf whole embryos. A specific diminution of the targeted transcripts for *col6a2* and *col6a4a* was detected: 5 and 8 % of WT, respectively (Fig. 3). These results were also confirmed by RT-qPCR on cDNA from 48hpf embryos (data not shown). Unfortunately, we failed to detect *col6a4b* transcripts by Northern blot at this stage, and by RT-qPCR in *col6a4b* mutants. We also investigated whether the knockdown of one of the genes affected the levels of the other transcripts. In *col6a2* morphants, *col6a4a* levels were slightly increased (163% of WT), while a 53% reduction in the levels of *col6a2* transcript was detected in *col6a4a* morphants (Fig. 3). By RT-qPCR, no significant variation in the levels of *col6a1* and *col6a3* were noted (data not shown).

Phenotypic alterations of col6a morphants

From 24hpf, *col6a2*, *col6a4a* and *col6a4b* morpholino-injected embryos displayed obvious macroscopic defects under light microscopy. As illustrated in Figure 4A, they present shorter and bent bodies, and vertical myosepta do not display the characteristic “chevron” shape seen in WT as well as in scramble MO-injected embryos; rather, myosepta of morphant embryos exhibited an abnormal “U-shape” curvature. These features are quite characteristic

of the knockdown of proteins involved in muscle development and/or myopathies. At 48hpf, more than 80% of *col6a* morpholino-injected embryos presented a slight developmental delay characterized by a reduced pigmentation and aberrant head-to-body angle (36), in addition to curved bodies and smaller eyes, phenotypes which are not observed in scramble MO-injected embryos. To assess muscle integrity, embryos were examined under polarizing light. Decreased birefringence was observed in all morphants compared to WT, indicating compromised muscle fibres organization (Fig. 4B). At the functional level, all morphants also exhibited an absence of escape response to touch stimulus, or uncoordinated movements, compared to WT and embryos injected with the scramble MO (Supplemental movies 1-5). It is worth mentioning that similar results were obtained when we injected donor splice site MOs (data not shown), with the exception of *col6a2* since the absence of a suitable sequence at the donor site prevented us from designing a morpholino. All *col6a* morphants died around 10dpf, most likely as a consequence of impaired motility which prevented them from feeding after yolk sac exhaustion (data not shown). As reported in other studies, morpholino injections yielded some phenotypic heterogeneity; nevertheless, *col6a* morphants mostly displayed distinctive muscle phenotypes, compared to scramble MO-injected embryos (Fig. 4C). All morphants used in the following experiments were sorted, so that “monster” morphants were discarded.

Phenotypic rescue of col6a2 morphants by co-injection with col6a2 RNA

To confirm that the phenotype observed in *col6a2* morphants was indeed specific to the knockdown of *col6a2*, zebrafish *col6a2* RNA was co-injected with the *col6a2*-MO, leading to more than 85% of co-injected embryos with a phenotype similar to WT, and restored motility (Fig. 5A, B and Supplemental movie 6). Quantitative RT-PCR demonstrated that *col6a2* transcript levels in co-injected embryos were restored to levels comparable to WT (Fig. 5C).

On the other hand, co-injection of *col6a2* RNA with the *col6a4a*-MO failed to rescue the phenotype of morphants (Fig. S4A, B), although *col6a2* transcript levels were indeed increased (Fig. S4C). As anticipated, *col6a4a* transcripts were not modulated in co-injected embryos (data not shown). Unfortunately, similar experiments could not be performed for the *col6a4* morphants due to the large size of the corresponding cDNAs that impeded their cloning.

Altered myofibrils and myotome boundaries components

In light of the macroscopic alterations induced by the down-regulation of *col6a* genes, we further examined the muscle structure by immunostaining on whole embryos. At 48hpf, dystrophin, a sub-sarcolemmal protein, correctly accumulated to myotome boundaries in WT embryos as well as morphants, but this staining appeared slightly irregular and less defined in the latter, and revealed misshapen myotome boundaries, particularly in *col6a2*-MO injected embryos, and to a lesser extent in *col6a4* morphants (Fig. 6). Collagen type XXII (COLXXII), a recently described MTJ marker (37), was also investigated, further demonstrating the abnormal shape of myosepta. COLXXII staining appeared to be most affected upon down-regulation of *col6a2*, and to a lesser degree in *col6a4* morphants (Fig. 6). Staining with an antibody against slow myosin revealed that in all morphants the labelled myofibres spanned entire somites, as in WT embryos, although they were less closely packed, possibly due to lateral detachment that appears as gaps between fibres. On the contrary, WT muscle fibres were tightly connected to each other along their length. These defects were still visible in embryos at 5dpf (Fig. 6).

Muscle structure and ultrastructural analysis of 5dpf zebrafish muscle

To further examine the effects of *col6a2*, and both *col6a4* knockdown on muscle structure, semi-thin sections were stained with toluidine blue (Fig. 7A). Light microscopy revealed the regular pattern of myofibrils and the fine, straight vertical myosepta in WT embryos. On the contrary, muscle fibers were clearly disorganized in *col6a2* morphants, with abundant undifferentiated sarcoplasm, large nuclei and their enlarged nucleoli. The knock-down of *col6a4a* did not alter the muscle structure while in *col6a4b* morphants, vacuolar areas were visible between myocytes. At the ultrastructural level, WT myofibrils presented the characteristic mature regular organization, with triads aligned with Z disks (Fig. 7B). The down-regulation of the two *col6a4* genes did not alter significantly the sarcomeric organization, although some vacuolated areas are present at the myocyte periphery in *col6a4b* morphant muscle. On the contrary, *col6a2* morphant muscle was severely disorganized with ill-defined Z bands, enlarged T-tubules but no sarcoplasmic reticulum dilatation (arrows in Fig. 7B). In addition, large undifferentiated sarcoplasmic areas with altered mitochondria were also observed. These mitochondria showed an increased matrix electrodensity, an enlarged space between their outer and inner membranes and a pronounced cristae swelling. As described above, vertical myosepta were affected by the down-regulation of all *col6a* genes. In WT embryos, the regular and thin myosepta, which contained a dense matrix of collagen fibril bundles were outlined by the electron-dense sarcolemma and subsarcolemma and by the continuous, less electron-dense, lamina densa of the basement membrane (Fig. 7C). *Col6a4a* morphant septa also showed a continuous basement membrane and a dense collagen network, but appeared wider and more ramified than in controls. In sharp contrast, *col6a2* and *col6a4b* morphant myosepta were drastically altered; they were highly enlarged with discontinuous remnants of basal lamina bordering a vacuolated and nearly empty matrix

with sparse collagen bundles. Moreover, *col6a4b* myosepta specifically exhibited quite irregular boundaries, with short additional ramifications (Insets in Fig. 7C).

The ultrastructure of the triangular zone of intersection between vertical septum and skin also showed the same type of alterations in *col6a2* and *col6a4b* morphants (Fig. S5). While in WT and MO-*col6a4a* triangles, a characteristic orthogonally-arranged, dense collagen stroma linked the deep **epidermal** surface and underlying myocytes, *col6a2* and *col6a4b*-deficient triangles appeared disorganized and vacuolated, with sparse and loose collagen fibrils attached to the **epidermis**.

It must be noted that the devastated aspect of *col6a2* and *col6a4b*-deficient septa and triangles suggests a particularly loose organization of their collagenous matrix, which could have less resisted dehydration and embedding procedures.

Altered $\alpha 2(VI)$ expression in *col6a4* morphants

We developed a specific antibody against zebrafish $\alpha 2$ chain, which proved useful in Western Blotting experiments. The antibody detects a band at the appropriate size in protein extracts from adult WT zebrafish muscle and from 72 hpf whole embryos. The specificity of this antibody was assessed by immunogenic peptide competition, which abolished the detection of the bands (Fig. 8A). The levels of $\alpha 2$ were drastically decreased in embryos injected with MO- $\alpha 2$, as expected, but also in extracts from the *col6a4* morphants (Fig. 8B).

Pathophysiological mechanisms

Since increased apoptosis had previously been reported in *col6a1* morphants (38), we examined whether this was also the case in the 3 morphants, by wholemount immunostaining of active caspase 3, a late marker of the apoptotic pathway. We observed a non-specific

increase in the number of positive cells in the hindbrain, most likely due to the micro-injections themselves, as it was also detected with the scramble MO. On the other hand, some specific signal was visible in the trunk region of the different *col6a* morphants, in particular in *col6a4b* morphants (Fig. 9A).

Defective induction of autophagy has been implicated in the pathogenesis of COLVI-miopathies, in a murine model of $\alpha 1$ deficiency, as well as in biopsies and cultured cells from patients (39, 40). Since a number of genes involved in this clearance mechanism are conserved in zebrafish (41), we investigated the levels of membrane-associated LC3 (LC3II) by Western blotting and showed that they were decreased in all *col6a* morphants (Fig. 9B). This reduced LC3 conversion thus points to an alteration in autophagosome formation, an early step of autophagy. We also assessed whether *col6a* knockdown affected Akt signalling, a pivotal actor in numerous biological processes, including cell survival and autophagy (42-44). Reduced Akt activity (*i.e.* its phosphorylation) has previously been shown in muscle of *Col6a1*-null mice (39). Phospho-Akt/total Akt ratios tend to be decreased in *col6a2* and *col6a4a* morphants, and even more so in *col6a4b* morphants, although statistical significance was not reached (Fig. 9B).

Neuronal outgrowth defects

In addition to the muscle defects detailed above, wholemount immunostaining with the SV2 antibody that labels synaptic vesicles revealed abnormal motor axons outgrowth in the 3 morphants: *col6a2* and *col6a4a* deficient embryos frequently displayed no or very short ventral axons, while *col6a4b* morphants presented axons with hyperbranching (Fig. 10A). The severity of these defects was ranked according to the extent of growth with respect to the horizontal myoseptum, and to the degree of branching (following the scoring described in (45); Fig. 10B). Overall, up to 40% of *col6a2* and *col6a4a* deficient embryos displayed the

most severe defects in motor axons outgrowth, classified as scores 0 and 1 (*i.e.* no growth or growth arrest before the horizontal myoseptum). On the contrary, over half of *col6a4b* morphants presented motor axons that grew beyond the horizontal myoseptum but were abnormally branched (score 2). To further understand these defects, we investigated whether *hdac6*, a microtubule-associated histone deacetylase involved in migration processes (46, 47), was differentially expressed upon *col6a* knockdown. Quantitative qPCR revealed that *hdac6* transcripts levels were significantly reduced in *col6a2* morphants only (Fig. 10C). This reduction was alleviated upon co-injection with *col6a2* RNA, as were motor axons growth defects (Fig. 10C and data not shown).

Discussion

Although a significant proportion of patients with neuromuscular phenotypes reminiscent of COLVI-related disorders do not harbour mutations in the *COL6A1-3* genes, no mutations have been reported in the human *COL6A5* or *COL6A6* genes to date.

In this study, we identified two zebrafish orthologs of the recently described $\alpha 4$, $\alpha 5$ and $\alpha 6$ chains, whose discovery has increased the complexity of collagen VI (11, 14, 20). Phylogenetic and domain structure analyses led us to name the corresponding genes *col6a4a* and *col6a4b*, in light of their higher homology with murine $\alpha 4$ and the presence of Kunitz domains, which are present only in $\alpha 3$ and in murine $\alpha 4$ (14, 48). Of note, in databases, a partial sequence of *col6a4a* had been computationally predicted as *col6a6* from the zebrafish genome assembly, as were most of other fish *col6a4* genes. This is most likely due to automated annotation of genome sequencing in reference to human genome in which the *COL6A4* gene is rearranged. Another argument supporting the fact that zebrafish *col6a4a* is indeed part of the *col6a4-a6* group is the presence on chromosome 16 of a small region of synteny (*pik3r4-col6a4*) with human chromosome 3 (*PIK3R4-COL6A6-COL6A5*), mouse

chromosome 9 (*Pik3r4-Col6a6-Col6a5-Col6a4*) and chicken chromosome 2 (*pik3r4-col6a4*). According to the phylogenetic tree, one evolutionary hypothesis would imply a *col6a4* ancestor gene that underwent duplication in fish (as did many genes in the teleost genomes (49)), giving rise to *col6a4a* and *col6a4b* that evolved differently. This ancestor gene may have been triplicated in mammalian, on the same chromosome, and corresponds to the *Col6a4-6* genes (11). In *Xenopus tropicalis* the presence of two genes, which C-terminal sequences allow clustering in two different groups may support this hypothesis and be a landmark of these later duplication events. Indeed one of these frog genes is closer to *Col6a4* in tetrapods and slow evolving fish (*Latimeria chalumnae* and *Callorhinchus milii*) while the second gene is clearly grouped with the mammalian *Col6a5-6* cluster. The grouping by pairs of *Col6a4* genes in *Latimeria chalumnae* and *Callorhinchus milii* is not explained but may be related to the fact that their genomes have been identified as very slow evolving ones (50, 51).

We first characterized the temporal expression of *col6a4a* and *col6a4b* during zebrafish development. We showed a distinctive expression kinetic pattern for *col6a4b*, which appears delayed compared to that of *col6a4a* and the other long-chain encoding gene *col6a3*. The *col6a1/a2* genes, encoding the 2 short chains, are expressed at higher levels throughout zebrafish development, in agreement with the requirement of $\alpha 1$ and $\alpha 2$ for assembly of heterotrimers with all the long chains. Using *in situ* hybridization, *col6a4a/b* transcripts could be detected in myotome, as well as in the eye, where mammalian COLVI is known to be expressed (4, 52-54). Interestingly, while the murine $\alpha 4$ protein is not expressed in muscle, $\alpha 5$ and $\alpha 6$ are differentially expressed in skeletal muscle. In humans, $\alpha 5$ is specifically detected at the myotendinous junction (MTJ), while $\alpha 6$ is mainly interstitial with partial co-localization with $\alpha 3$ (29). In addition, $\alpha 5$ shows a unique, strong expression at the basal lamina of neuromuscular junctions (NMJ) and at the perineurium of intramuscular peripheral nerves

(14, 55). Indeed, one remaining question is whether zebrafish $\alpha 4a$ and $\alpha 4b$ may functionally be assimilated to mammalian $\alpha 5$ and $\alpha 6$.

We created models of $\alpha 4a$ and $\alpha 4b$ deficiency in zebrafish, using an anti-sense strategy against *col6a4a* and *col6a4b*. In parallel, we also targeted the *col6a2* gene, to model loss of function of one of the chains involved in COLVI-related myopathy. The splice site MO used here led to a truncated protein with a PTC occurring before the TH domain, and degradation of the corresponding mRNA. The resulting muscle phenotype was very similar to that obtained upon in-frame skipping of zebrafish *col6a1* exon 9 (corresponding to human exon 10) as reported by Telfer *et al.* (38). Importantly, knockdown of *col6a4a* and *col6a4b* also caused muscle disorganization and dysfunction: all morphants displayed abnormal trunk curvature, misshapen vertical myosepta, defects in muscle organization and ultrastructure, leading to reduced motility. Although *col6a4b* transcript levels were very low in early developmental stages, the corresponding morphants displayed a clear muscle phenotype. One hypothesis for this apparent contradiction could be that early on *col6a4b* expression is restricted to as of yet unidentified territories where it could play a crucial role for muscle development

Collectively these results confirm the essential function(s) of all COLVI proteins in zebrafish muscle development. Since MOs remain active during approximately 5 days, we assessed whether a phenotype reversion could be obtained thereafter. This was not the case since morphant larvae died after yolk exhaustion, likely due to their inability to fetch food owing to the severe motility defects seen as early as 24hpf.

Overall, *col6a2* morphants presented the most severe muscle phenotype, a consequence of the ubiquitous expression of the $\alpha 2$ chain, and its presence in all monomers. Interestingly, *col6a4a* and *col6a4b* morphants displayed some specific phenotypes, with the latter showing a more pronounced muscle dysfunction as evidenced by birefringence and ME

analyses. On the other hand, motoneuron axonal growth was more severely impaired in *col6a4a* and *col6a2* morphants.

Over the last 10 years, numerous studies on *Col6a1* knock-out mice have provided some clues on pathogenic mechanisms in skeletal muscle. In particular, increased apoptosis and defective autophagy, have been described in this animal model (39, 40, 56-58). The former was also reported in *col6a1* MO-induced zebrafish models (38, 59, 60). Here, we assessed caspase-3 expression in *col6a2*, *col6a4a* and *col6a4b* morphants but did not detect a major increase in the number of apoptotic cells. Of note, no apoptosis could be detected in the recently described *Col6a3* mutant mice either, nor in human biopsies suggesting that apoptosis may not be a universal mechanism involved in the mediation of COLVI defects. Autophagy being a conserved process in zebrafish (41), we investigated whether COLVI-deficiency had any effect on its early stages (*i.e.* autophagosome formation and/or elongation), by analogy to the murine *Col6a1*^{-/-} findings. Similarly, we detected lower levels of the lipidated form of LC3 (LC3II) in all morphants; furthermore, beclin 1 levels, another factor involved in the autophagic process, also tended to be reduced (data not shown). One important mediator of muscle homeostasis is Akt/PKB, which is activated upon phosphorylation, and plays a regulatory role on autophagy (43). In *Col6a1*^{-/-} mice, prolonged starvation (>24h) enabled autophagy induction, but this type of experiment cannot be carried out in zebrafish larvae since nutrients are provided by the yolk sac. In fed *Col6a1*^{-/-} mice, levels of activated Akt do not differ from those in WT mice, while upon starvation they are increased in *tibialis anterior* muscle, but not in diaphragm, suggesting a muscle type-specific response to nutrient depletion (39). In protein extracts from whole *col6a2* and *col6a4b* morphants, we detected reduced levels of the activated form of Akt, while they were not altered in *col6a4a* morphants. This finding may reflect the rather mild muscle structure alterations in the latter model compared to the other two.

The importance of ECM molecules in axon guidance has been previously reported in zebrafish. For example, COLXV-deficient embryos present primary motoneurons guidance defects similar to those observed in the morphants presented here (61). In the *col6a* morphants presented here, the SV2 staining appeared weak and diffuse, which may indicate a defect of nicotinic acetylcholine receptor focalisation, a process that is dependent on axonal growth (62). Furthermore, the importance of COLVI has already been demonstrated in neural crest development (63). Recently, nerve conduction defects and delayed response to acute pain stimuli have been described in *Col6a1*^{-/-} mice. Indeed, COLVI is expressed by Schwann cells and its deficit leads to hypermyelination of peripheral nervous system (64). How the primary neuron growth defects might relate (*i.e.* cause or consequence) to the muscle phenotypes remains to be determined in *col6a* morphants. The decrease in *hdac6* expression does appear specific and may contribute to the neuronal outgrowth defects, as previously shown in Amyotrophic Lateral Sclerosis (65, 66). Of interest, somewhat similar axonal growth defects were very recently reported in new *col6a3* zebrafish models reproducing mutations identified in patients with dystonia (67).

Collectively, our data point to the zebrafish $\alpha 4a$ and $\alpha 4b$ -encoding genes as being similar to an ancestor gene for vertebrate $\alpha 4-6$. In mammals, this ancestor gene has likely been triplicated into *Col6a4-6*. The expression pattern of zebrafish *col6a4* and *col6a2* genes overlap, and the kinetics of expression of zebrafish *col6a4* suggest a role for these genes during muscle development and transient inactivation supports this hypothesis. Finally, the phenotypes observed in zebrafish *col6a4* morphants strongly support the hypothesis that deficiency in COLVI-chains other than $\alpha 1-3$ may also lead to muscle dysfunction, and warrant screening of the human *COL6A5* and/or *COL6A6* genes in neuromuscular phenotypes of unknown aetiology.

Material and Methods

Zebrafish strains and maintenance

Different strains (AB, TU, ABC) were used for this study, with no difference in the experimental data obtained. They were kept at 28°C with a 14 hour light cycle, using standard maintenance protocols. Animal care and experimentation were performed in compliance with French and European laws.

Sequence and phylogenetic analyses

COLVI phylogeny was performed using domains C-terminus to the collagen motif. The ClustalX software was used to perform the alignment and phylogeny (Neighbor-Joining method). The phylogenetic tree was drawn using FigTree v1.4.0. The same tree was obtained using the domains Nterminus to the collagen motif (data not shown).

In situ hybridization

Larvae were fixed overnight at 4°C in 4% PFA then progressively dehydrated in methanol and stored in 100% methanol at -20°C. Fragments of cDNA were produced by PCR targeting regions 5' to the collagenic domain (Fig. 1B). Amplified fragments were cloned in pGEM-T (Promega) according to the supplier instructions. Clones suitable to produce antisense probes with T7 RNA polymerase (Roche) were selected and probes purified after synthesis using mini Quick Spin RNA columns (Roche).

Whole-mount *in situ* hybridizations (ish) were performed according to the protocol described in (68) with modifications as described in Zfin (<https://wiki.zfin.org>). Hybridized probes were revealed using anti-DIG antibody coupled to AP (Roche) and staining was obtained with NBT and BCIP (Roche). After staining, larvae were fixed overnight in 4% PFA then washed in

PBSTw, transferred to glycerol at progressively increasing concentration and stored in 100% glycerol. Lateral and dorsal views were imaged in depression slides in 100% glycerol under dissecting microscope (SZX9 Olympus) using DFK 31AU03 camera and IC Capture software (both The Imaging Source).

For section ish, larvae fixed as above were progressively rehydrated and transferred in 30% sucrose then OCT medium (CellPath, CML). Larvae were transferred in mold (CML) and frozen in liquid nitrogen-chilled isopentane. Ten μm sections were performed using a CMS1510S cryostat (Leica) and left to dry at room temperature. Ish were performed according to (69) at 65°C in humid chambers. After staining, sections were covered with Mowiol and a coverslip. Images were obtained using a microscope (BX41 Olympus), DMK31AU03 camera and IC Capture software (both The Imaging Source).

In vitro transcription

The full length *col6a2* coding sequence was amplified from cDNA obtained from whole embryos by PCR using the Kapa HiFi ReadyMix (Kapabiosystems), then cloned into pGEM-t vector. RNA was synthesized from 1 μg of linearized *col6a2* plasmid using the AmpliCap-Max T7 High Yield Message Maker Kit (Epicentre Biotechnologies) following the manufacturer's instructions. Quantity and quality of the *col6a2* RNA were assessed on agarose gel.

Morpholinos and micro-injections:

Anti-sense morpholino oligonucleotides (MOs, Gene Tools LLC) targeted to interfere with *col6a2* (MO-a2; 5' ACTCTCTGAAGGGACAGAACACACT 3'), *col6a4a* (MO-a4a; 5' TACACCTGGGCATGATACAAAAGGA 3') and *col6a4b* (MO-a4b; 5' GACCCCTGGTTTACAAATCAGACAT 3') were designed over intron-exon junctions 1, 11

and 12, respectively. A mismatch (scramble) MO (scr; 5' ACTCTGTCAACGGACACAAGACT 3') with no sequence homology in the zebrafish genome was used as a control. MOs were dissolved in distilled water at a concentration of 500 μ M along with 0.1% phenol red, which served as a positive marker for successful injections. Fertilized eggs were injected at the 1-2 cell stage with approximately 3-4 ng of MO. For the rescue experiment, *col6a2* mRNA (100ng/ μ l) was co-injected with the MO-a2. Injected embryos and non-injected controls were placed in a 28°C incubator to recover and euthanized with a lethal dose of benzocaine at various stages depending on the experiments.

Live image analysis

Embryos were photographed at 24 and 48 hpf using a Leica MZ8 Stereomicroscope. Embryos were embedded in methylcellulose to prevent movements.

RNA extraction and first strand cDNA synthesis

RNA was extracted from whole embryos at different stages with the RNeasy Fibrous Tissue Mini Kit (Qiagen) according to the manufacturer's instructions. RNA yield and quality were assessed with the Nanodrop system (Thermo Scientific). cDNAs were synthesized from 500 ng of RNA with oligo dT primers using the SuperScript III First-Strand Synthesis System for RT-PCR (Invitrogen), following the manufacturer's instructions.

Northern Blot

Northern blot analysis was carried out as previously described (70). Briefly, 8 μ g of total RNA were separated on 1.3 % agarose/MOPS-gels containing 0.66 M formaldehyde and transferred overnight onto Hybond-N+ membrane (Amersham Pharmacia Biotech) by capillarity with 10x SSC. Blots were hybridized with random-primed ³²P-labeled probes

(from PCR amplicons; about 300 nucleotide-long) in a hybridization buffer (2 % SDS, 10 % dextran sulfate, 1 x SSPE, 100 µg/ml salmon sperm DNA, 2 % Denhart's) at 68°C overnight. Signals were analyzed on a phospho-imager (Molecular Imager FX, Bio-Rad). Probe sequences are available upon request.

RT-quantitative PCR

RT-qPCR was performed on a Light Cycler 480 System (Roche) using the LighCycler480 SYBR Green I Master mix (Roche) with specific primers for *col6a1-a4b*. The program included an initial denaturation step of 8 min at 95°C, followed by 50 amplification cycles of 10 sec denaturation at 95°C for, 15 sec hybridization at 58°C, and 15 sec elongation at 72°C. Data were normalized to the expression levels of the elongation factor alpha I (*elfa*), a housekeeping gene whose expression is acceptably stable throughout zebrafish development (71). Primers sequences are available upon request.

Birefringence

Muscle birefringence was analyzed by placing living 48hpf embryos in 3% methylcellulose under an Olympus BX41 microscope with a DMK 31AU03 camera using IC Capture software (both The Imaging Source).

Escape test

48hpf embryos were subjected to a tactile stimulus: using a clamp, a gentle stimulus was applied at the extremity of the larvae tail and its reaction was recorded with an Olympus SZX9 microscope with a DMK 31AU03 camera using the IC Capture software (both from The Imaging Source).

Zebrafish $\alpha 2(VI)$ antibody synthesis

We obtained a polyclonal antibody against the zebrafish $\alpha 2$ chain from Interchim/Abgent. The C-terminal sequence RLTLAQGDDDERNAR was identified as the most immunogenic and specific peptide. It was injected (5-8 times) in rabbits and the serum obtained and purified with affinity or protein A purification. Competition experiments on Western Blotting were performed to verify the specificity of the antibody. Briefly, purified polyclonal rabbit anti-zebrafish COLVI antibody (diluted 1:250 in blocking solution) was incubated with 500 μ g (250 fold more) of the purified immunogenic peptide overnight at 4°C. Subsequently, Western Blotting was performed and the signal was efficiently extinguished.

Whole mount immunocytochemistry

Embryos were dechorionated at 48hpf, euthanized with benzocaine and either directly stocked in RNA later or fixed in 4% paraformaldehyde, dehydrated and stored in 100% MetOH. Immunostaining was carried out on whole embryos with the following antibodies: anti slow myosin (F59; DSHB; 1:20), anti-dystrophin (MANDRA1; Sigma; 1:1000), anti-COLXXII (a gift from F. Ruggiero, Lyon, France; 1:250), anti-synaptic vesicle protein 2 (SV2, DSHB, 1:100). For apoptosis assessment, anti-cleaved caspase3 (559565, BD Pharmingen; 1:100) was used. Alexa Fluor secondary antibodies (goat anti-mouse A568, goat anti-rabbit A488; Jackson ImmunoResearch) were incubated at 1:1000 for 1 hour at room temperature. Embryos were rinsed and mounted in 100% glycerol. Images were obtained under an Axiophot microscope (Zeiss) and images were captured using the Metaview software (Ropper Scientific) or on a confocal microscope (Olympus FV-1000).

Western Blot

Total proteins from 72hpf embryos were extracted using extraction buffer (0.2M NaCl, 0.1M Glycine, 0.1% Triton, 50 μ M DTT, 10mM EDTA, 20mM Tris pH 7.5, 2% protease inhibitors and 2% phosphatase inhibitors). Fifty μ g of these proteins were separated using 10% or 8-16% gradient gels for 4 to 5 hours at 100V at room temperature. They were then transferred on PVDF 0.45 μ m membranes overnight, at 600mA and 4°C. Membranes were blocked in 5% skim milk/PBS for 1 hour and then hybridized overnight at 4°C with primary antibodies against LC3, Akt, P-Akt^{Ser} (Cell Signalling) and α 2(VI). Then, they were washed 3x 15 min with 1% skim milk/PBS-Tween and hybridized with appropriate HRP-conjugated secondary antibodies (Jackson ImmunoResearch) for 1 hour at room temperature. Membranes were washed again and revealed using the Immobilon Western chemiluminescent HRP substrate (Millipore) on the chemi-imager G-box (Syngene).

Electron Microscopy

Embryos were anaesthetized with benzocaine, immediately immersed in 2.5% glutaraldehyde in PBS during 2 hours, rinsed 3 times in PBS and finally stored in PBS at 4°. After a 2% OsO₄ 40 min fixation, they were gradually dehydrated in acetone including a 1% uranyl staining step in 70% acetone, and finally flat embedded in Epon resin (EMS, Fort Washington, PA, USA). 500nm parasagittal semi-thin sections were stained with 1% toluidine blue. After uranyl and lead citrate staining, parasagittal 70nm ultrathin sections were examined with a Philips CM120 electron microscope (Philips, Eindhoven, The Netherlands) operated at 80kV and photographed with a SIS Morada digital camera (Olympus Soft Imaging Solutions GmbH, Münster, Germany).

Statistical analysis:

Data are means \pm SD. ANOVA tests were performed to determine significant differences between groups. When normality or equal variance test failed, a Kruskal-Wallis One Way analysis was used. All tests were performed using SigmaStat (Systat, Erkrath, Germany).

Accession numbers

Accession numbers of sequences used in this study were as follows: Mouse (*Mus musculus*) *Col6a1* NP_034063.1, *Col6a2* NP_666119.1, *Col6a3* NP_001229937.1, *Col6a4* NP_081039.2, *Col6a5* NP_001161395.1, *Col6a6* NP_001096077.1; Human (*Homo sapiens*) *COL6A1* NP_001839.2, *COL6A2* NP_001840.3, *COL6A3* NP_004360.2, *COL6A5* NP_001265227.1, *COL6A6* NP_001096078.1; Zebrafish (*Danio rerio*) *col6a1* XP_009304444.1, *col6a2* XP_696164.2, *col6a3* XP_009302963.1, *col6a6* XP_692457.6, *col28a1* NP_001153314.1; Rat (*Rattus norvegicus*) *Col6a4* NP_001258111.1, *Col6a5* XP_008756121.1, *Col6a6* XP_008764827.1; Marmoset (*Callithrix jacchus*), *Col6a4* XP_002759734.1, *Col6a5* XP_008982098.1, *Col6a6* XP_002759733.2; Frog (*Xenopus (Silurana) tropicalis*) *col6a1* XP_002932077.2, *col6a2* NP_001120436.1, *col6a3* XP_002932067.2, *col6a6_1* XP_002937788.2, *col6a6_2* XP_002942405.2; chicken (*Gallus gallus*) *Col6a1* NP_990438.1, *Col6a2* NP_990679.1, *Col6a3* NP_990865.1, *Col6a4* XP_426008.4; Medaka (*Oryzias latipes*) *col6a1* XP_004079144.1, *col6a2a* XP_004079072.1, *col6a2b* XP_004081925.1, *col6a3* XP_004078593.1; African coelacanth (*Latimeria chalumnae*) *col6a1* XP_005997002.1, *col6a2* XP_006014655.1, *col6a3* XP_005997469.1, *col6a6a* XP_006004266.1, *col6a6b* XP_006010064.1; Elephant shark (*Callorhynchus milii*) *col6a1* XP_007898245.1, *col6a2* XP_007896379.1, *col6a3* XP_007904071.1, *col6a6a* XP_007887867.1, *col6a6b* XP_007887975.1; half-smooth tongue sole (*Cynoglossus semilaevis*) *col6a1* XP_008332498.1, *col6a2* XP_008326809.1, *col6a3* XP_008327160.1,

col6a6 XP_008321223.1; dog (*Canis lupus familiaris*) *col6a1* XP_003434049.2, *col6a2* XP_005639077.1, *col6a3* NP_001096685.1, *col6a4* XP_853242.2, *col6a5* XP_853265.3, *col6a6* XP_853279.3; northern pike (*Esox lucius*) *col6a1* XP_010863420.1, *col6a2* XP_010865210.1, *col6a3* XP_010865851.1, *col6a4* XP_010903537.1.

Author Contributions

LR, XC and VA conceived and designed the experiments. LR, CR, JL, AK, LJ, CG and MF performed experiments. LR, CR, JL, AK, XC and VA analysed the data. LR, JL, XC and VA wrote the paper. LL was responsible for fish maintenance. EK and SC provided zebrafish embryos and access to the ICM facility.

All authors have read and approved submission of this work.

Funding

This work was supported by the Institut National de la Santé et de la Recherche Médicale (Inserm), the Association Française contre les Myopathies (AFM), the Sorbonne Universités – UPMC, and the Centre National de la Recherche Scientifique (CNRS).

Acknowledgments

We are grateful to Dr Sylvie Schneider-Maunoury (UPMC, Paris, France) for providing some zebrafish embryos in the course of this study and for discussions. We thank Dr Florence Ruggiero (Institut de Génomique Fonctionnelle de Lyon, France) for the gift of the COLXXII antibody and for discussions. We are thankful to Dr Malika Kapsimali (Ecole Nationale Supérieure de Paris, France) for expert advice. We acknowledge the Plate-forme d'Imagerie Cellulaire Pitié-Salpêtrière for image acquisition on confocal microscope. The F59 and SV2 antibodies developed by Frank E. Stockdale (Stanford University School of Medicine,

Stanford, CA) and Kathleen M. Buckley (Harvard Medical School, Boston, MA), respectively, were obtained from the Developmental Studies Hybridoma Bank created by the NICHD of the NIH and maintained at The University of Iowa, Department of Biology, Iowa City, IA 52242.

Conflict of Interest Statement

None declared

References

- 1 Ricard-Blum, S. (2011) The collagen family. *Cold Spring Harb. Perspect. Biol.*, **3**, a004978.
- 2 Bonaldo, P., Russo, V., Bucciotti, F., Doliana, R. and Colombatti, A. (1990) Structural and functional features of the alpha 3 chain indicate a bridging role for chicken collagen VI in connective tissues. *Biochem.*, **29**, 1245-1254.
- 3 Burg, M.A., Tillet, E., Timpl, R. and Stallcup, W.B. (1996) Binding of the NG2 proteoglycan to type VI collagen and other extracellular matrix molecules. *J. Biol. Chem.*, **271**, 26110-26116.
- 4 Doane, K.J., Yang, G. and Birk, D.E. (1992) Corneal cell-matrix interactions: type VI collagen promotes adhesion and spreading of corneal fibroblasts. *Exp. Cell Res.*, **200**, 490-499.
- 5 Heino, J. (2007) The collagen family members as cell adhesion proteins. *BioEssays*, **29**, 1001-1010.
- 6 Keene, D., Engvall, E. and Glanville, R. (1988) Ultrastructure of type VI collagen in human skin and cartilage suggests an anchoring function for this filamentous network. *J. Cell Biol.*, **107**, 1995-2006.
- 7 Kuo, H.-J., Maslen, C.L., Keene, D.R. and Glanville, R.W. (1997) Type VI Collagen Anchors Endothelial Basement Membranes by Interacting with Type IV Collagen. *J. Biol. Chem.*, **272**, 26522-26529.
- 8 McDevitt, C.A., Marcelino, J. and Tucker, L. (1991) Interaction of intact type VI collagen with hyaluronan. *FEBS Lett.*, **294**, 167-170.
- 9 Pfaff, M., Aumailley, M., Specks, U., Knolle, J., Zerwes, H.G. and Timpl, R. (1993) Integrin and Arg-Gly-Asp Dependence of Cell Adhesion to the Native and Unfolded Triple Helix of Collagen Type VI. *Exp. Cell Res.*, **206**, 167-176.
- 10 Wiberg, C., Klatt, A.R., Wagener, R., Paulsson, M., Bateman, J.F., Heinegard, D. and Morgelin, M. (2003) Complexes of matrilin-1 and biglycan or decorin connect collagen VI microfibrils to both collagen II and aggrecan. *J. Biol. Chem.*, **278**, 37698-37704.
- 11 Fitzgerald, J., Holden, P. and Hansen, U. (2013) The expanded collagen VI family: new chains and new questions. *Connect. Tissue Res.*, **54**, 345-350.
- 12 Colombatti, A., Bonaldo, P., Ainger, K., Bressan, G.M. and Volpin, D. (1987) Biosynthesis of chick type VI collagen. I. Intracellular assembly and molecular structure. *J. Biol. Chem.*, **262**, 14454-14460.
- 13 Engvall, E., Hesse, H. and Klier, G. (1986) Molecular assembly, secretion, and matrix deposition of type VI collagen. *J. Cell Biol.*, **102**, 703-710.
- 14 Gara, S.K., Grumati, P., Urciuolo, A., Bonaldo, P., Kobbe, B., Koch, M., Paulsson, M. and Wagener, R. (2008) Three Novel Collagen VI Chains with High Homology to the {alpha}3 Chain. *J. Biol. Chem.*, **283**, 10658-10670.
- 15 Baldock, C., Sherratt, M.J., Shuttleworth, C.A. and Kielty, C.M. (2003) The supramolecular organization of collagen VI microfibrils. *J. Mol. Biol.*, **330**, 297-307.
- 16 Ball, S., Bella, J., Kielty, C. and Shuttleworth, A. (2003) Structural Basis of Type VI Collagen Dimer Formation. *J. Biol. Chem.*, **278**, 15326-15332.
- 17 Chu, M., Conway, D., Pan, T., Baldwin, C., Mann, K., Deutzmann, R. and Timpl, R. (1988) Amino acid sequence of the triple-helical domain of human collagen type VI. *J. Biol. Chem.*, **263**, 18601-18606.
- 18 Engel, J., Furthmayr, H., Odermatt, E., von der Mark, H., Aumailley, M., Fleischmajer, R. and Timpl, R. (1985) Structure and macromolecular organization of type VI collagen. *Ann N.Y. Acad. Sci.*, **460**, 25-37.

- 19 Furthmayr, H., Wiedemann, H., Timpl, R., Odermatt, E. and Engel, J. (1983) Electron-microscopical approach to a structural model of intima collagen. *Biochem J*, **211**, 303-311.
- 20 Fitzgerald, J., Rich, C., Zhou, F.H. and Hansen, U. (2008) Three Novel Collagen VI Chains, $\{\alpha\}4(VI)$, $\{\alpha\}5(VI)$, and $\{\alpha\}6(VI)$. *J. Biol. Chem.*, **283**, 20170-20180.
- 21 Nakajima, M., Miyamoto, Y. and Ikegawa, S. (2011) Cloning and characterization of the osteoarthritis-associated gene DVWA. *J. Bone Miner. Metab.*, **29**, 300-308.
- 22 Wagener, R., Gara, S.K., Kobbe, B., Paulsson, M. and Zaucke, F. (2009) The knee osteoarthritis susceptibility locus DVWA on chromosome 3p24.3 is the 5' part of the split COL6A4 gene. *Matrix Biol.*, **28**, 307-310.
- 23 Ullrich, O. (1930) Kongenitale, atonisch-sklerotische Muskeldystrophie, ein weiteres Typus der heredodegenerativen Erkrankungen des neuromuskulären Systems. *Z Gesamte Neurol Psychiat*, **126**, 171-201.
- 24 Bethlem, J. and Van Wijngaarden, G.K. (1976) Benign myopathy with autosomal dominant inheritance: a report of three pedigrees. *Brain*, **99**, 91-100.
- 25 Allamand, V., Brinas, L., Richard, P., Stojkovic, T., Quijano-Roy, S. and Bonne, G. (2011) ColVI myopathies: where do we stand, where do we go? *Skelet Muscle*, **1**, 30.
- 26 Bonnemann, C.G. (2011) The collagen VI-related myopathies Ullrich congenital muscular dystrophy and Bethlem myopathy. *Handb. Clin. Neurol.*, **101**, 81-96.
- 27 Lampe, A.K. and Bushby, K.M.D. (2005) Collagen VI related muscle disorders. *J Med Genet*, **42**, 673-685.
- 28 Sabatelli, P., Gara, S.K., Grumati, P., Urciuolo, A., Gualandi, F., Curci, R., Squarzone, S., Zamparelli, A., Martoni, E., Merlini, L. *et al.* (2011) Expression of the collagen VI alpha5 and alpha6 chains in normal human skin and in skin of patients with collagen VI-related myopathies. *J. Invest. Dermatol.*, **131**, 99-107.
- 29 Sabatelli, P., Gualandi, F., Gara, S.K., Grumati, P., Zamparelli, A., Martoni, E., Pellegrini, C., Merlini, L., Ferlini, A., Bonaldo, P. *et al.* (2012) Expression of collagen VI alpha5 and alpha6 chains in human muscle and in Duchenne muscular dystrophy-related muscle fibrosis. *Matrix Biol.*, **31**, 187-196.
- 30 Tagliavini, F., Pellegrini, C., Sardone, F., Squarzone, S., Paulsson, M., Wagener, R., Gualandi, F., Trabanelli, C., Ferlini, A., Merlini, L. *et al.* (2014) Defective collagen VI $\alpha 6$ chain expression in the skeletal muscle of patients with collagen VI-related myopathies. *Biochim. Biophys. Acta*, **1842**, 1604-1612.
- 31 Bassett, D. and Currie, P. (2003) The zebrafish as a model for muscular dystrophy and congenital myopathy. *Hum Mol Genet.*, **12**, R265-270.
- 32 Lieschke, G.J. and Currie, P.D. (2007) Animal models of human disease: zebrafish swim into view. *Nat. Rev. Genet.*, **8**, 353-367.
- 33 Steffen, L.S., Guyon, J.R., Vogel, E.D., Beltre, R., Pusack, T.J., Zhou, Y., Zon, L.I. and Kunkel, L.M. (2007) Zebrafish orthologs of human muscular dystrophy genes. *BMC Genomics*, **8**, 79.
- 34 Charvet, B., Malbouyres, M., Pagnon-Minot, A., Ruggiero, F. and Le Guellec, D. (2011) Development of the zebrafish myoseptum with emphasis on the myotendinous junction. *Cell Tissue Res.*, **346**, 439-449.
- 35 Stickney, H.L., Barresi, M.J. and Devoto, S.H. (2000) Somite development in zebrafish. *Dev. Dyn.*, **219**, 287-303.
- 36 Kimmel, C.B., Ballard, W.W., Kimmel, S.R., Ullmann, B. and Schilling, T.F. (1995) Stages of embryonic development of the zebrafish. *Dev. Dyn.*, **203**, 253-310.
- 37 Charvet, B., Guiraud, A., Malbouyres, M., Zwolanek, D., Guillon, E., Breaud, S., Monnot, C., Schulze, J., Bader, H.L., Allard, B. *et al.* (2013) Knockdown of *col22a1* gene in zebrafish induces a muscular dystrophy by disruption of the myotendinous junction. *Development*, **140**, 4602-4613.

- 38 Telfer, W.R., Busta, A.S., Bonnemann, C.G., Feldman, E.L. and Dowling, J.J. (2010) Zebrafish models of collagen VI-related myopathies. *Hum. Mol. Genet.*, **19**, 2433-2444.
- 39 Grumati, P., Coletto, L., Sabatelli, P., Cescon, M., Angelin, A., Bertaggia, E., Blaauw, B., Urciuolo, A., Tiepolo, T., Merlini, L. *et al.* (2010) Autophagy is defective in collagen VI muscular dystrophies, and its reactivation rescues myofiber degeneration. *Nat Med*, **16**, 1313-1320.
- 40 Grumati, P., Coletto, L., Schiavinato, A., Castagnaro, S., Bertaggia, E., Sandri, M. and Bonaldo, P. (2011) Physical exercise stimulates autophagy in normal skeletal muscles but is detrimental for collagen VI-deficient muscles. *Autophagy*, **7**, 1415-1423.
- 41 Fleming, A. and Rubinsztein, D.C. (2011) Zebrafish as a model to understand autophagy and its role in neurological disease. *Biochim. Biophys. Acta*, **1812**, 520-526.
- 42 Boppart, M.D., Burkin, D.J. and Kaufman, S.J. (2011) Activation of AKT signaling promotes cell growth and survival in alpha7beta1 integrin-mediated alleviation of muscular dystrophy. *Biochim. Biophys. Acta*, **1812**, 439-446.
- 43 Noguchi, M., Hirata, N. and Suizu, F. (2014) The links between AKT and two intracellular proteolytic cascades: ubiquitination and autophagy. *Biochim. Biophys. Acta*, **1846**, 342-352.
- 44 Wang, R.C., Wei, Y., An, Z., Zou, Z., Xiao, G., Bhagat, G., White, M., Reichelt, J. and Levine, B. (2012) Akt-mediated regulation of autophagy and tumorigenesis through Beclin 1 phosphorylation. *Science*, **338**, 956-959.
- 45 Sleigh, J.N., Barreiro-Iglesias, A., Oliver, P.L., Biba, A., Becker, T., Davies, K.E., Becker, C.G. and Talbot, K. (2014) Chondrolectin affects cell survival and neuronal outgrowth in in vitro and in vivo models of spinal muscular atrophy. *Hum. Mol. Genet.*, **23**, 855-869.
- 46 Hubbert, C., Guardiola, A., Shao, R., Kawaguchi, Y., Ito, A., Nixon, A., Yoshida, M., Wang, X.F. and Yao, T.P. (2002) HDAC6 is a microtubule-associated deacetylase. *Nature*, **417**, 455-458.
- 47 Li, Y., Shin, D. and Kwon, S.H. (2013) Histone deacetylase 6 plays a role as a distinct regulator of diverse cellular processes. *FEBS J.*, **280**, 775-793.
- 48 Chu, M.L., Zhang, R.Z., Pan, T.C., Stokes, D., Conway, D., Kuo, H.J., Glanville, R., Mayer, U., Mann, K., Deutzmann, R. *et al.* (1990) Mosaic structure of globular domains in the human type VI collagen alpha 3 chain: similarity to von Willebrand factor, fibronectin, actin, salivary proteins and aprotinin type protease inhibitors. *EMBOJ.*, **9**, 385-393.
- 49 Jaillon, O., Aury, J.M., Brunet, F., Petit, J.L., Stange-Thomann, N., Mauceli, E., Bouneau, L., Fischer, C., Ozouf-Costaz, C., Bernot, A. *et al.* (2004) Genome duplication in the teleost fish *Tetraodon nigroviridis* reveals the early vertebrate proto-karyotype. *Nature*, **431**, 946-957.
- 50 Amemiya, C.T., Alfoldi, J., Lee, A.P., Fan, S., Philippe, H., Maccallum, I., Braasch, I., Manousaki, T., Schneider, I., Rohner, N. *et al.* (2013) The African coelacanth genome provides insights into tetrapod evolution. *Nature*, **496**, 311-316.
- 51 Venkatesh, B., Lee, A.P., Ravi, V., Maurya, A.K., Lian, M.M., Swann, J.B., Ohta, Y., Flajnik, M.F., Sutoh, Y., Kasahara, M. *et al.* (2014) Elephant shark genome provides unique insights into gnathostome evolution. *Nature*, **505**, 174-179.
- 52 El-Shabrawi, Y., Kublin, C.L. and Cintron, C. (1998) mRNA levels of alpha1(VI) collagen, alpha1(XII) collagen, and beta ig in rabbit cornea during normal development and healing. *Invest. Ophthalmol. Vis. Sci.*, **39**, 36-44.
- 53 Myint, E., Brown, D.J., Ljubimov, A.V., Kyaw, M. and Kenney, M.C. (1996) Cleavage of human corneal type VI collagen alpha 3 chain by matrix metalloproteinase-2. *Cornea*, **15**, 490-496.

- 54 Takahashi, T., Cho, H.I., Kublin, C.L. and Cintron, C. (1993) Keratan sulfate and dermatan sulfate proteoglycans associate with type VI collagen in fetal rabbit cornea. *J Histochem Cytochem*, **41**, 1447-1457.
- 55 Gara, S.K., Grumati, P., Squarzone, S., Sabatelli, P., Urciuolo, A., Bonaldo, P., Paulsson, M. and Wagener, R. (2011) Differential and restricted expression of novel collagen VI chains in mouse. *Matrix Biol.*, **30**, 248-257.
- 56 Bernardi, P. and Bonaldo, P. (2013) Mitochondrial dysfunction and defective autophagy in the pathogenesis of collagen VI muscular dystrophies. *Cold Spring Harb. Perspect. Biol.*, **5**, a011387.
- 57 Irwin, W., Bergamin, N., Sabatelli, P., Reggiani, C., Megighian, A., Merlini, L., Braghetta, P., Columbaro, M., Volpin, D., Bressan, G. *et al.* (2003) Mitochondrial dysfunction and apoptosis in myopathic mice with collagen VI deficiency. *Nat. Genet.*, **35**, 367-371.
- 58 Maraldi, N.M., Sabatelli, P., Columbaro, M., Zamparelli, A., Manzoli, F.A., Bernardi, P., Bonaldo, P. and Merlini, L. (2009) Collagen VI myopathies: From the animal model to the clinical trial. *Adv. Enzyme Regul.*, **49**, 197-211.
- 59 Zulian, A., Tagliavini, F., Rizzo, E., Pellegrini, C., Sardone, F., Zini, N., Maraldi, N.M., Santi, S., Faldini, C., Merlini, L. *et al.* (2014) Melanocytes from Patients Affected by Ullrich Congenital Muscular Dystrophy and Bethlem Myopathy have Dysfunctional Mitochondria That Can be Rescued with Cyclophilin Inhibitors. *Front Aging Neurosci.*, **6**, 324.
- 60 Zulian, A., Rizzo, E., Schiavone, M., Palma, E., Tagliavini, F., Blaauw, B., Merlini, L., Maraldi, N.M., Sabatelli, P., Braghetta, P. *et al.* (2014) NIM811, a cyclophilin inhibitor without immunosuppressive activity, is beneficial in collagen VI congenital muscular dystrophy models. *Hum. Mol. Genet.*, **23**, 5353-5363.
- 61 Pagnon-Minot, A., Malbouyres, M., Haftek-Terreau, Z., Kim, H.R., Sasaki, T., Thisse, C., Thisse, B., Ingham, P.W., Ruggiero, F. and Le Guellec, D. (2008) Collagen XV, a novel factor in zebrafish notochord differentiation and muscle development. *Dev. Biol.*, **316**, 21-35.
- 62 Behra, M., Cousin, X., Bertrand, C., Vonesch, J., Biellmann, D., Chatonnet, A. and U, S. (2002) Acetylcholinesterase is required for neuronal and muscular development in the zebrafish embryo. *Nat Neurosci.*, **5**, 111-118.
- 63 Perris, R., Kuo, H.J., Glanville, R.W. and Bronner-Fraser, M. (1993) Collagen type VI in neural crest development: distribution in situ and interaction with cells in vitro. *Dev. Dyn.*, **198**, 135-149.
- 64 Chen, P., Cescon, M., Megighian, A. and Bonaldo, P. (2014) Collagen VI regulates peripheral nerve myelination and function. *FASEB J.*, **28**, 1145-1156.
- 65 Fiesel, F.C., Voigt, A., Weber, S.S., Van den Haute, C., Waldenmaier, A., Gorner, K., Walter, M., Anderson, M.L., Kern, J.V., Rasse, T.M. *et al.* (2010) Knockdown of transactive response DNA-binding protein (TDP-43) downregulates histone deacetylase 6. *EMBO J.*, **29**, 209-221.
- 66 Schmid, B., Hruscha, A., Höggl, S., Banzhaf-Strathmann, J., Strecker, K., van der Zee, J., Teucke, M., Eimer, S., Hegermann, J., Kittelmann, M. *et al.* (2013) Loss of ALS-associated TDP-43 in zebrafish causes muscle degeneration, vascular dysfunction, and reduced motor neuron axon outgrowth. *Proc Natl Acad Sci U S A*, **110**, 4986-4991.
- 67 Zech, M., Lam, Daniel D., Francescato, L., Schormair, B., Salminen, Aaro V., Jochim, A., Wieland, T., Lichtner, P., Peters, A., Gieger, C. *et al.* Recessive Mutations in the $\alpha 3$ (VI) Collagen Gene *COL6A3* Cause Early-Onset Isolated Dystonia. *Am. J. Hum. Genet.*, in press.
- 68 Thisse, C. and Thisse, B. (2008) High-resolution in situ hybridization to whole-mount zebrafish embryos. *Nat. Prot.*, **3**, 59-69.

- 69 Redon, E., Bosseboeuf, A., Rocancourt, C., Da Silva, C., Wincker, P., Mazan, S. and Sourdain, P. (2010) Stage-specific gene expression during spermatogenesis in the dogfish (*Scyliorhinus canicula*). *Reproduction*, 140, 57-71.
- 70 Francois, V., Klein, A.F., Beley, C., Jollet, A., Lemerrier, C., Garcia, L. and Furling, D. (2011) Selective silencing of mutated mRNAs in DM1 by using modified hU7-siRNAs. *Nat Struct Mol Biol.*, 18, 85-87.
- 71 McCurley, A.T. and Callard, G.V. (2008) Characterization of housekeeping genes in zebrafish: male-female differences and effects of tissue type, developmental stage and chemical treatment. *BMC Mol. Biol.*, 9, 102.

Figure legends

Figure 1: Evolutionary analysis of COLVI chains, and organization of the $\alpha 2$, $\alpha 4a$ and $\alpha 4b$ proteins and corresponding transcripts.

(A) COLVI phylogeny was performed using domains C-terminus to the triple helical domain. The ClustalX software was used to perform the alignment and phylogeny (Neighbor-Joining method). The phylogenetic tree was drawn using FigTree v1.4.0. Numbers above nodes indicate their robustness (after 1000 bootstrap replications). Only nodes present in more than 75% of the trees (score of 0.75) are indicated. Except for zebrafish, the name indicated for protein is the one used in NCBI entries, this explained why most of fish Col6a4 proteins are named Col6a6 (see text).

Cj: *Callithrix jacchus*; Cl: *Canis lupus*; Cm: *Callorhinchus milii*; Cs: *Cynoglossus semilaevis*; Dr: *Danio rerio*; El: *Esox lucius*; Gg: *Gallus gallus*; Hs: *Homo sapiens*; Lc: *Latimeria chalumnae*; Mm: *Mus musculus*; Ol: *Oryzias latipes*; Rn: *Rattus norvegicus*; Xt: *Xenopus tropicalis*

(B) Schematic representation of the *col6a4a* and *col6a4b* coding sequences, as well as $\alpha 4a$ and $\alpha 4b$ chain structures. Green indicates signal peptide, red refers to triple helical regions (TH), globular vWFA domains are in blue, and Kunitz domains are depicted in orange. Translation initiation and termination sites are indicated above the diagrams. Morpholino oligonucleotides targeting acceptor splice sites are represented by yellow horizontal lines, and the ensuing premature termination codons by red hexagones. ISH probes are indicated by purple triangles above the schematics. Not drawn to scale.

(C) Schematic representation of the *col6a2* coding sequence and corresponding $\alpha 2(VI)$ chain structure. The *col6a2* non-coding exon is in purple. Morpholino oligonucleotide targeting acceptor splice site is represented by a yellow horizontal line, and the resulting premature

termination codon by a red hexagone. Position of the probe used for ISH and the peptide used to generate the $\alpha 2$ -specific antibody are noted as a purple triangle and a brown symbol, respectively. Not drawn to scale.

Figure 2: Kinetics of expression of zebrafish *col6* genes and spatial expression pattern of the *col6a2*, *col6a4a* and *col6a4b* genes.

(A) Temporal mRNA expression of *col6* genes during zebrafish development. Relative quantification of *col6a* transcript levels, normalized to the 48 hpf stage. Data are presented as means \pm SD of 3 qPCR experiments. * $p < 0.05$

(B) Spatial expression of *col6a2*, *col6a4a* and *col6a4b* genes in WT zebrafish embryos.

Whole mount *in situ* hybridization is shown at 48hpf (a, b, f, g, k, l) and 5dpf (c-e, h-j, m-o).

Larvae are in lateral (a, c-d, f, h-i, k, m-n) and dorsal view (b, e, g, j, l, o): anterior to the *left*, and dorsal is *up*. Black arrowheads point to pectoral fin buds (b, i), and pectoral fins (f, m, t).

White arrowheads indicate the sclera. Black arrows point to lens. Black asterisks refer to cornea. sc: spinal chord.

Figure 3: Transcript levels in *col6a2* and *col6a4a* morphants

Total RNA extracted from WT and MO-injected zebrafish (48hpf) were resolved and analysed by Northern blotting. Membranes were hybridized with random-primed ^{32}P -labeled specific probes (300 nt) and signals revealed on a phosphor-imager. Elfa1 was used as loading control. Densitometry of each band was performed using the ImageJ software, and the morphant/WT ratios are indicated below the corresponding blots.

Figure 4: Morphological alterations in morpholino-injected *col6a2*, *col6a4a* and *col6a4b* zebrafish embryos

(A) WT and morpholino-injected embryos in methylcellulose were observed under white light at 24 and 48hpf. White arrows in insets indicate vertical myosepta that present the characteristic chevron shape in WT and scramble (scr) MO-injected embryos, while they are abnormal in those injected with the 3 acceptor splice-site MOs.

(B) Birefringence analysis of WT and MO-injected embryos at 48hpf.

Dorso-lateral views are shown in (A) and (B): anterior to the *left*, and dorsal is *up*.

(C) Phenotypic repartition of WT (n=489), and MO-injected embryos (n=211, 148, 142 and 130 for MO-scr, a2, a4a and a4b, respectively) at 48hpf. Blue: no phenotype; Green: monster-like phenotype; Red: distinctive muscle phenotype.

Figure 5: Phenotypic rescue of *col6a2* morphants with *col6a2* mRNA

(A) Phenotype repartition of 48hpf WT embryos (n=142), WT injected with *col6a2* RNA alone (RNA-a2; n=77), *col6a2* MO-injected embryos (MO-a2; n=96), and embryos co-injected with the MO and *col6a2* RNA (MO-a2 + RNA-a2; n=223).

(B) Morphology analysis under light microscopy at 48hpf. The right panel is a magnified view of trunk showing the rescued muscle structure.

(C) Quantification of *col6a2* transcripts by specific RT-qPCR in 48hpf WT embryos (n=142), WT injected with *col6a2* RNA alone (RNA-a2), *col6a2* MO-injected embryos (MO-a2), and embryos co-injected with the MO and 100ng of *col6a2* RNA (MO-a2 + RNA-a2). Data are represented as arbitrary units ($E^{-\Delta C_t}$). Data are presented as means \pm SD of 3 experiments. * p<0.05.

Figure 6: Altered myofibrils and myotome boundaries in *col6a* morphants

Immunostaining for dystrophin (a-d), COLXXII (e-h), and slow myosin (i-p) were carried out on 48hpf (a-l) and 5dpf (m-p) whole embryos. Lateral gaps between myofibers are indicated by white arrows. Scale bars: 50 μ m except for i- l: 10 μ m

Figure 7: Skeletal muscle structure and ultrastructure of 5 dpf WT and *col6a* morphants

(A) Semi-thin sections showing the optical aspect of a hemi-myotome. Arrowheads indicate large nuclei with their enlarged nucleoli. Bar: 20 μ m.

(B) Sarcomeric ultrastructure. Triads are noted with arrows. Asterisks indicate large undifferentiated sarcoplasmic areas, with swollen mitochondria (M). Arrowheads point to vacuolated areas at the myocyte periphery. Bar: 1 μ m.

(C) Vertical myosepta are pseudo-colored in green. In all images, a dotted zone of the septum is enlarged in the inset below. N: nucleus. Bars: 2 μ m for the main images and 200nm for insets.

Figure 8: Altered α 2(VI) chain expression in *col6a* morphants

(A) Total protein extracts from adult WT zebrafish muscle and whole WT 72hpf embryos were separated by SDS-PAGE. PVDF membranes were hybridized with the specific anti- α 2(VI) antibody (left panel). Competition with the antigenic peptide abolished the detection of the α 2(VI) band (right panel).

(B) Total proteins extracted from 72hpf embryos were transferred to PVDF membranes, which were hybridized with the specific anti- α 2(VI) antibody. A portion of the same membrane stained with Ponceau S Red prior to hybridization is shown as a loading control.

Figure 9: Assessment of pathophysiological mechanisms in *col6a* morphants

(A) Wholemound immunostaining using an antibody against active caspase-3, in the head (left panel) and trunk (right panel) regions of 48hpf embryos. E: eye. Bars: 50 μ m

(B) Total protein extracted from 72hpf embryos were transferred to PVDF membranes, which were subsequently hybridized with antibodies against the membrane-associated form of LC3 (LC3II), the phosphorylated form of Akt (P-Akt^{Ser347}), and total Akt. A portion of the same membrane stained with Ponceau S Red before the hybridization is shown as a loading control.

Figure 10: Abnormal motor axon growth upon down-regulation of *col6a* genes

(A) Wholemound Sv2 immunolabeling to visualize presynaptic axons were performed on 48hpf WT and *col6a* knockdown embryos. Lateral views are presented with anterior side to the left and dorsal side up. Sc: spinal cord. Asterisks (*) indicate axons that did not grow beyond the hemi-segment line (score 1); white arrows point to axons with increased lateral branching (score 2). Scale bars: 50 μ m.

(B) Schematic of motor axon scoring according to the classification of Sleigh (45) and genotype repartition. (0): hemisegment without a ventral motor axon; (1): hemisegment with ventral motor axon that extended maximum to the horizontal myoseptum; (2): hemisegment with a ventral motor axon that had grown beyond the horizontal myoseptum and bifurcated, and had abnormal additional branching or failed to stay on the mid-segmental pathway; (3): hemisegment with a ventral motor axon as in WT.

(C) Quantification of *hdac6* transcript levels by RT-qPCR in 5dpf WT embryos, *col6a2* MO-injected embryos (MO-a2), embryos co-injected with the MO and 100ng of *col6a2* RNA (MO-a2 + RNA-a2), *col6a4a* and *col6a4b*-MO injected embryos (MO-a4a and MO-a4b, respectively). Data are represented as arbitrary units ($E^{-\Delta C_t}$). Data are means \pm SD of 4 qPCR experiments performed from 2 independent pools of RNA. * $p < 0.05$.

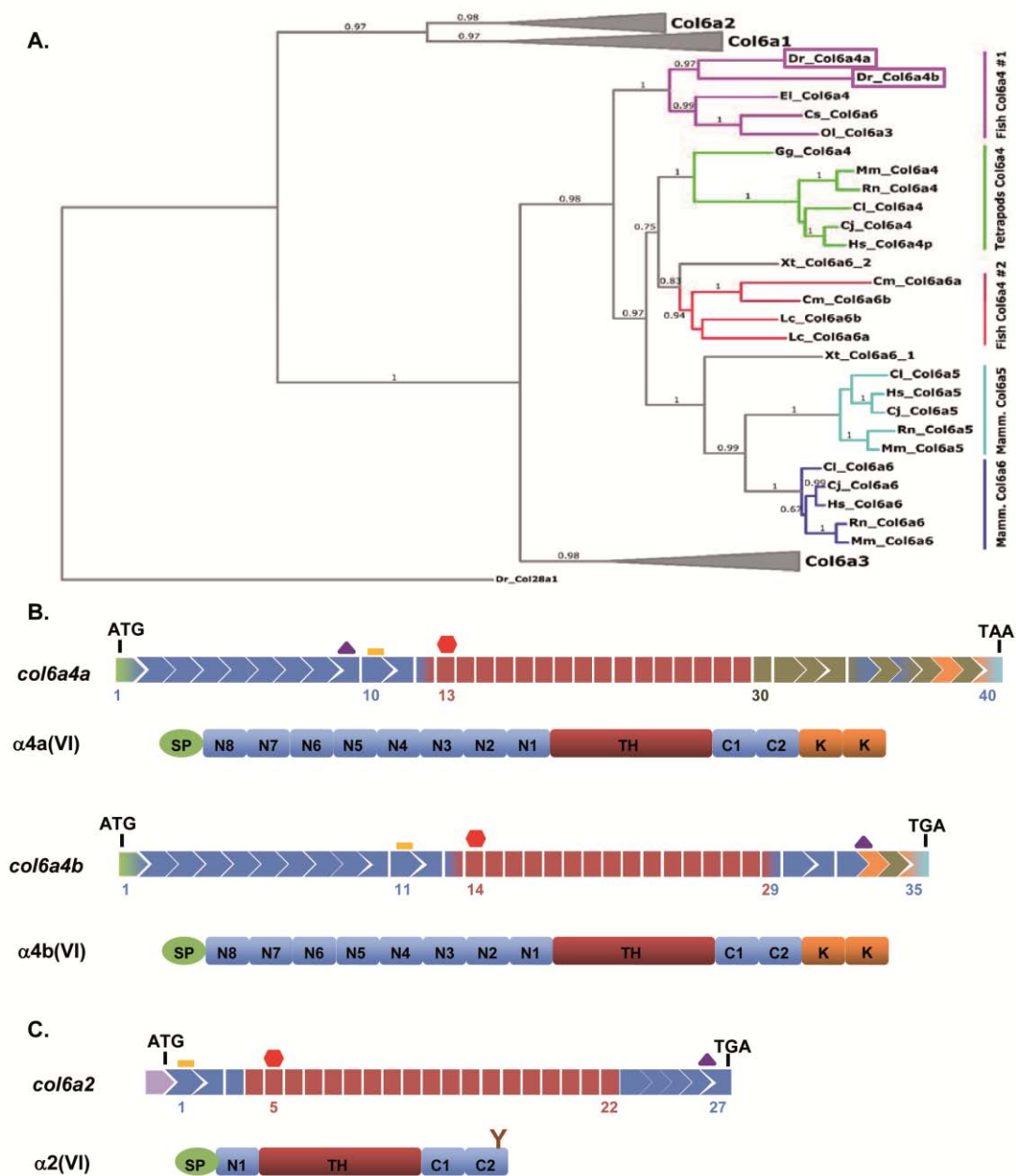
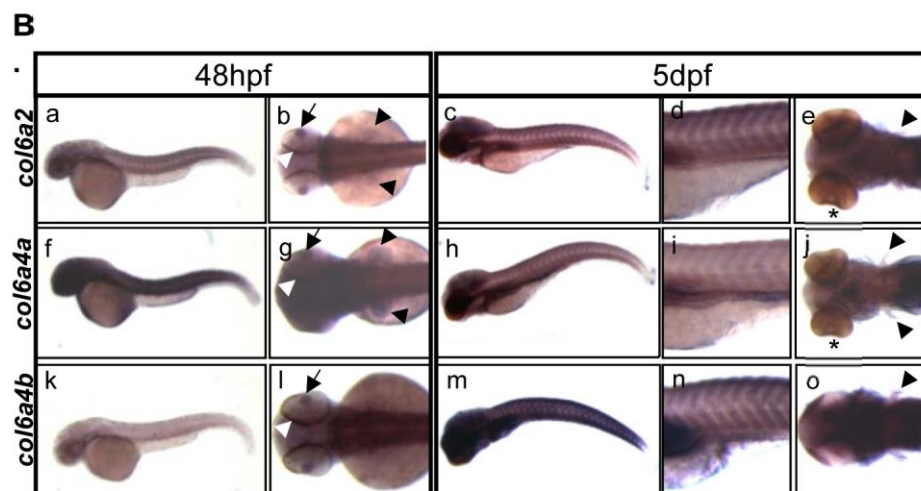
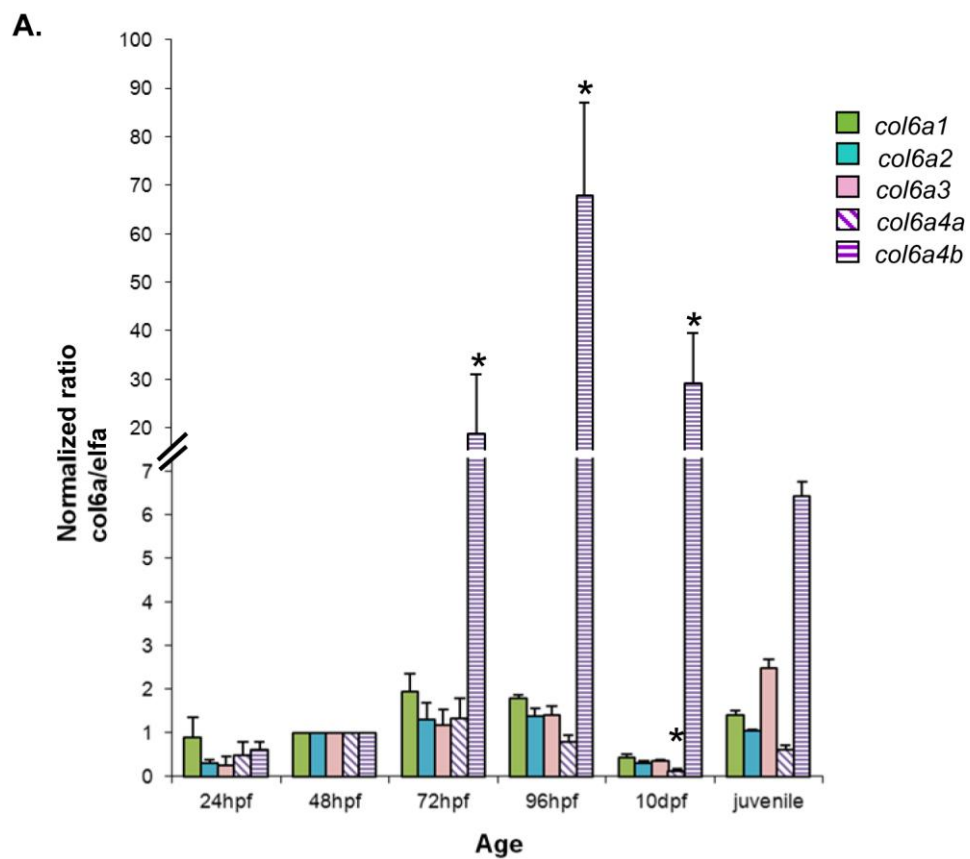


Figure 1



Revised Figure 2

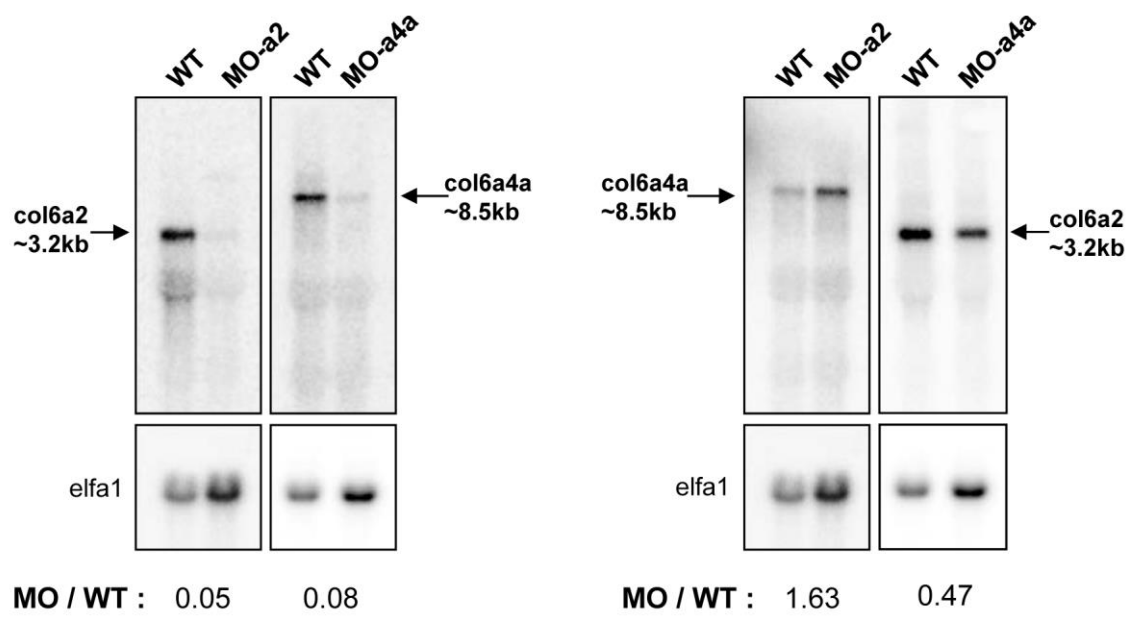


Figure 3

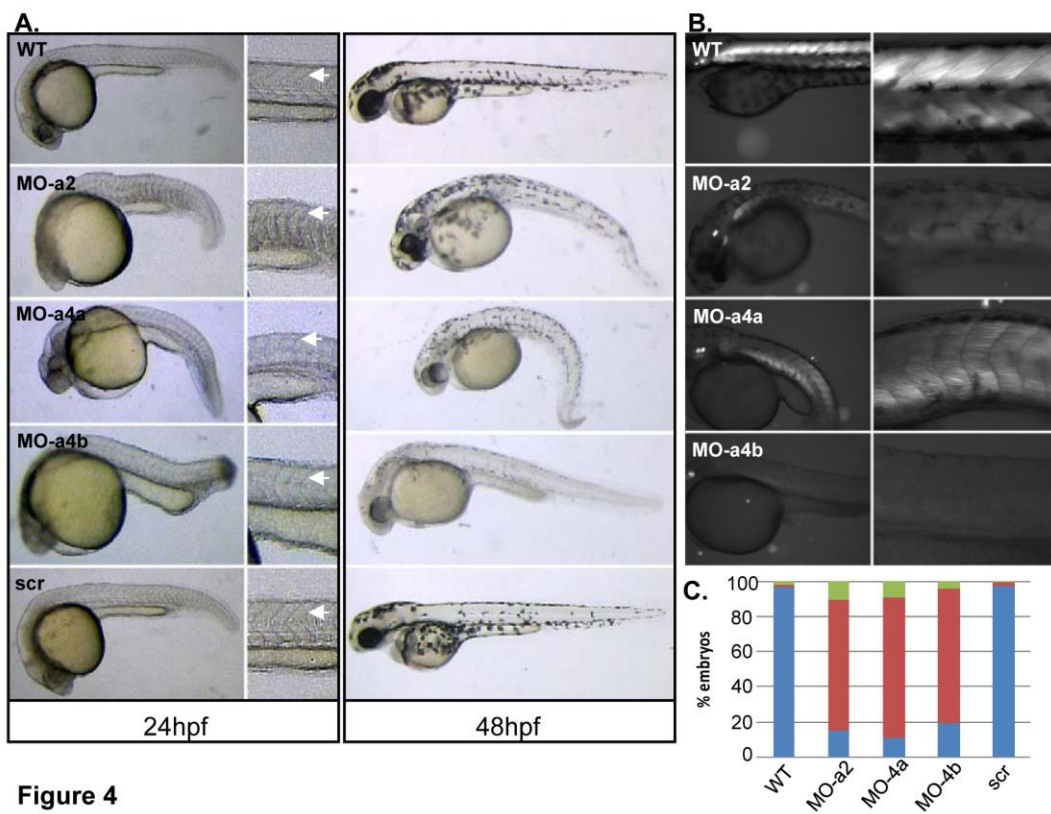


Figure 4

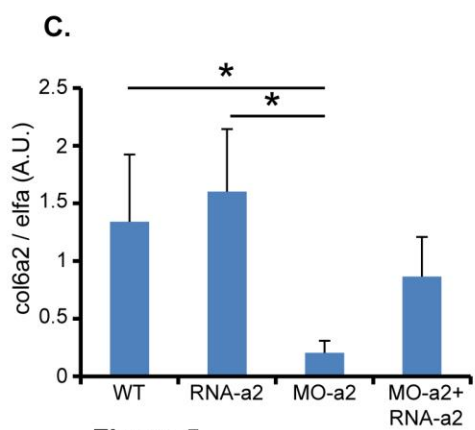
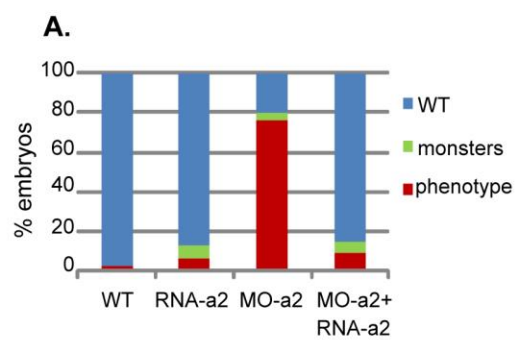
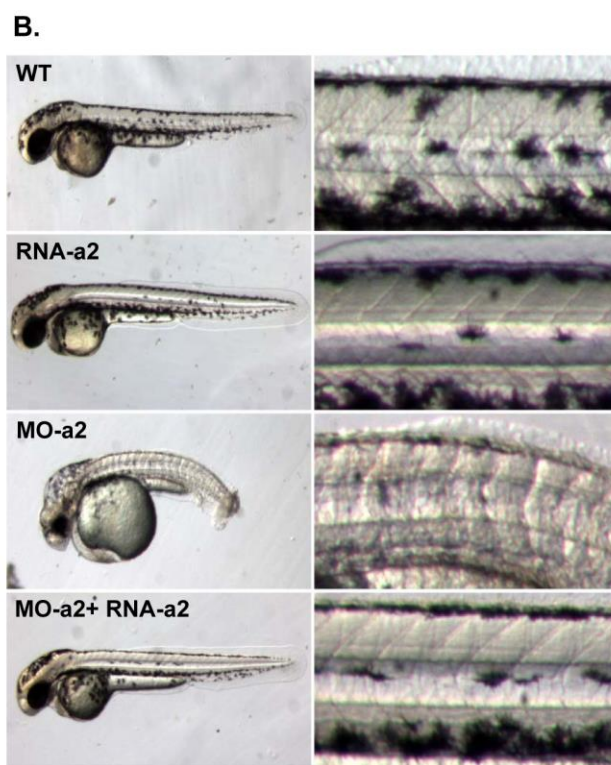


Figure 5



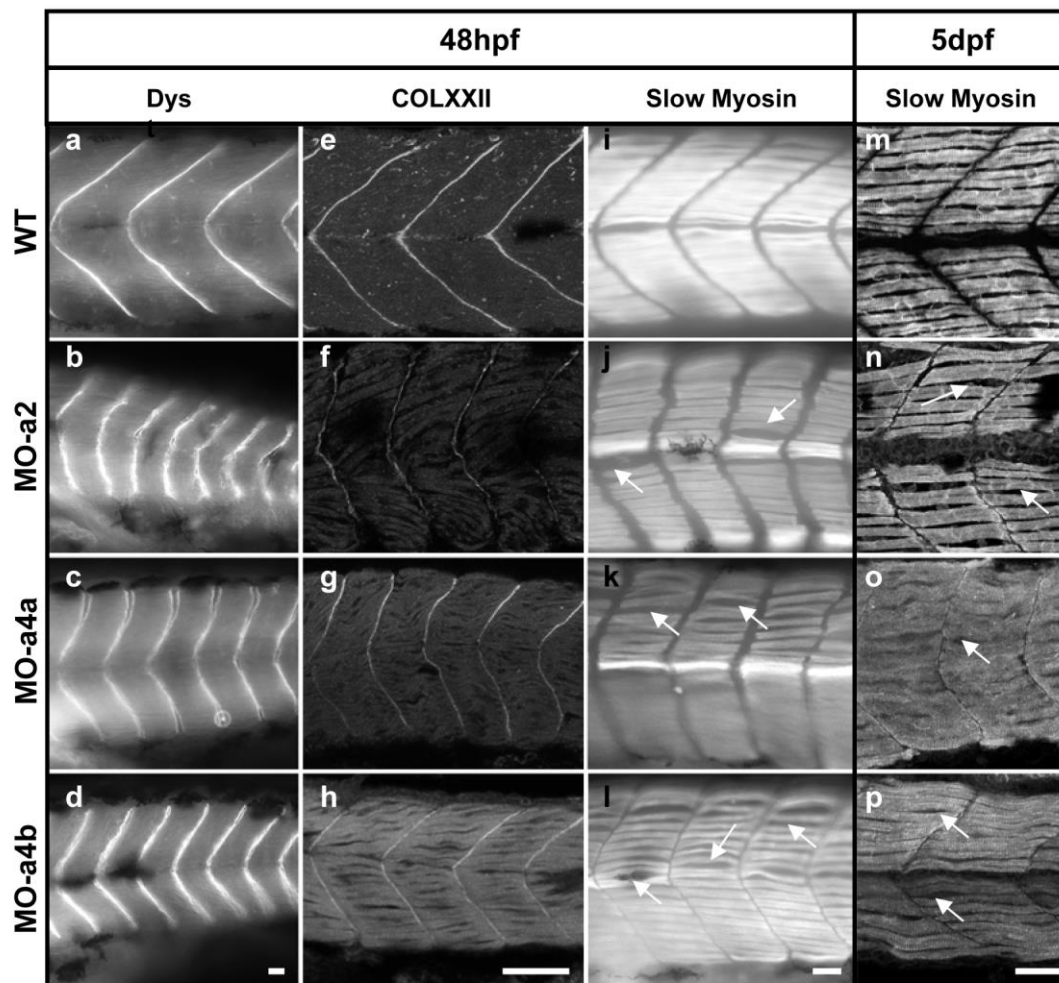
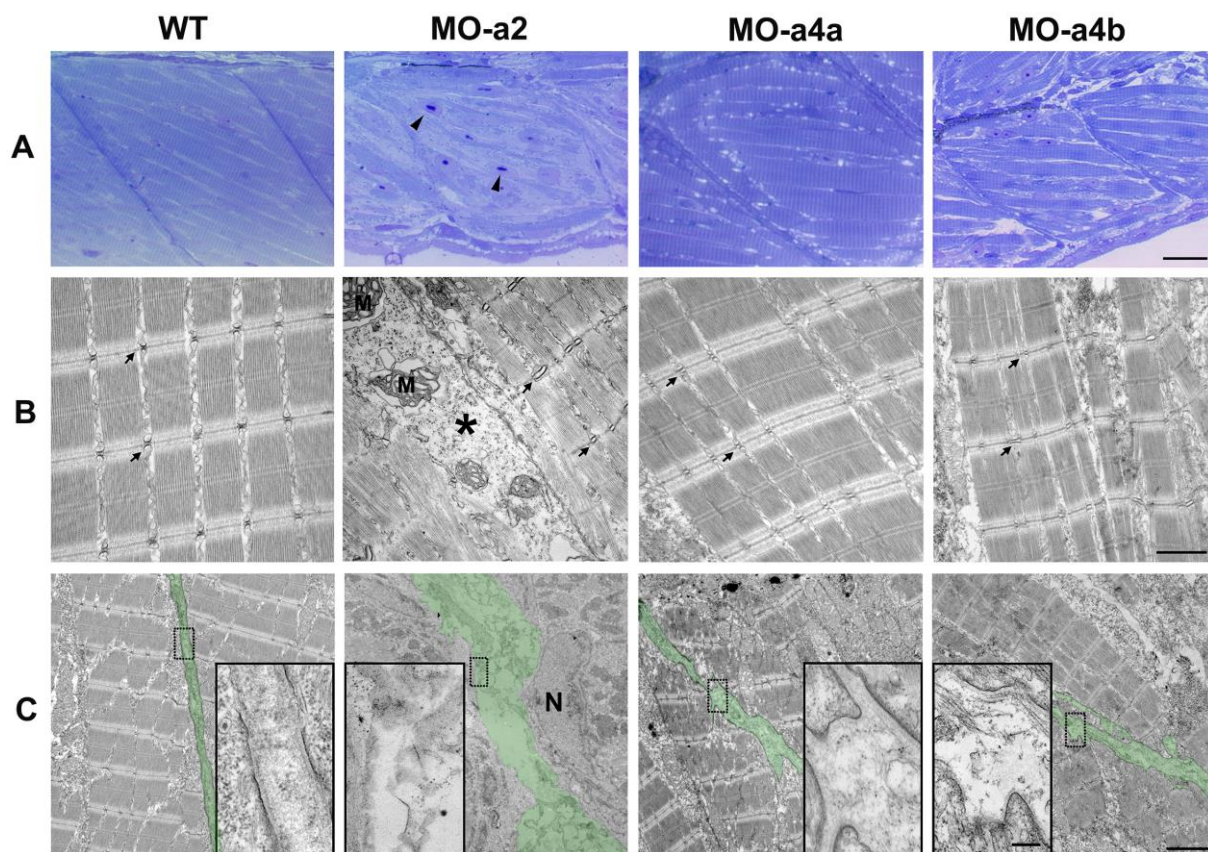


Figure 6



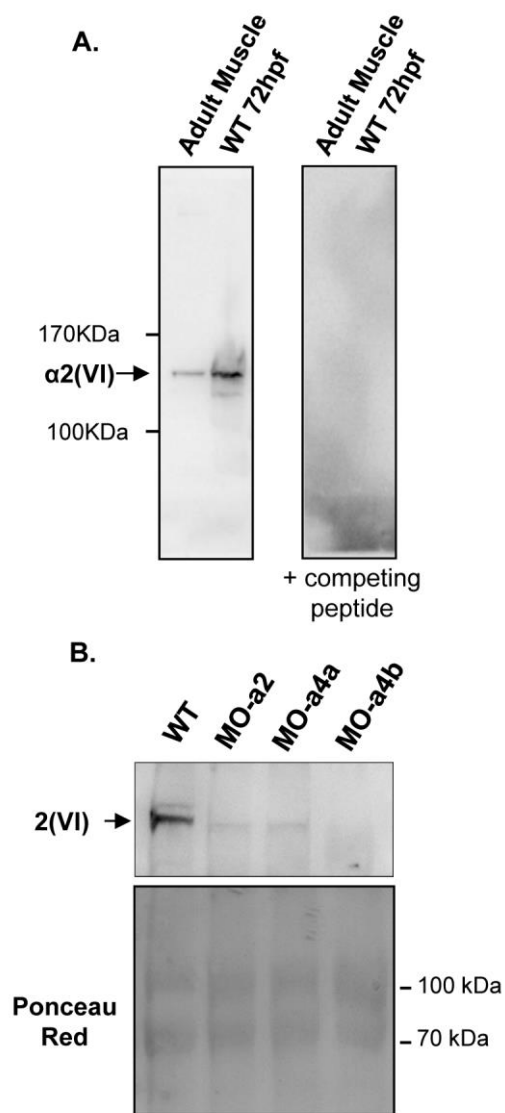


Figure 8

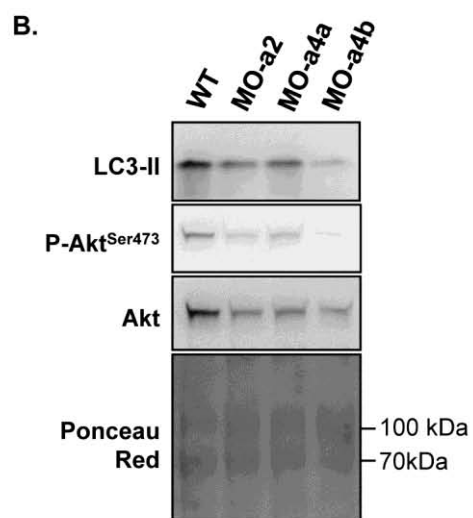
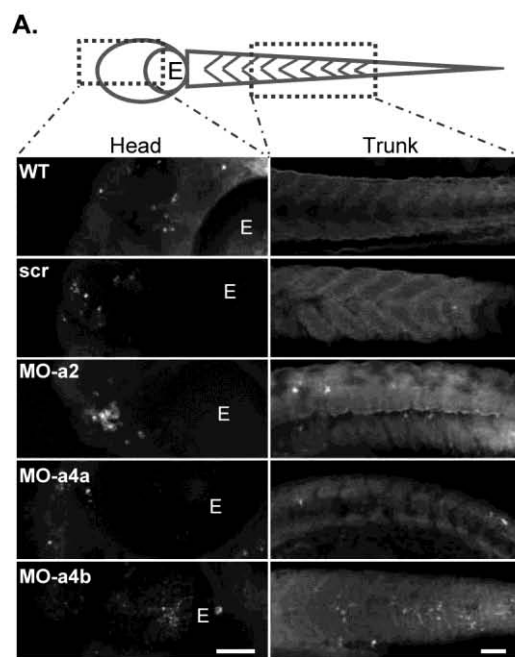


Figure 9

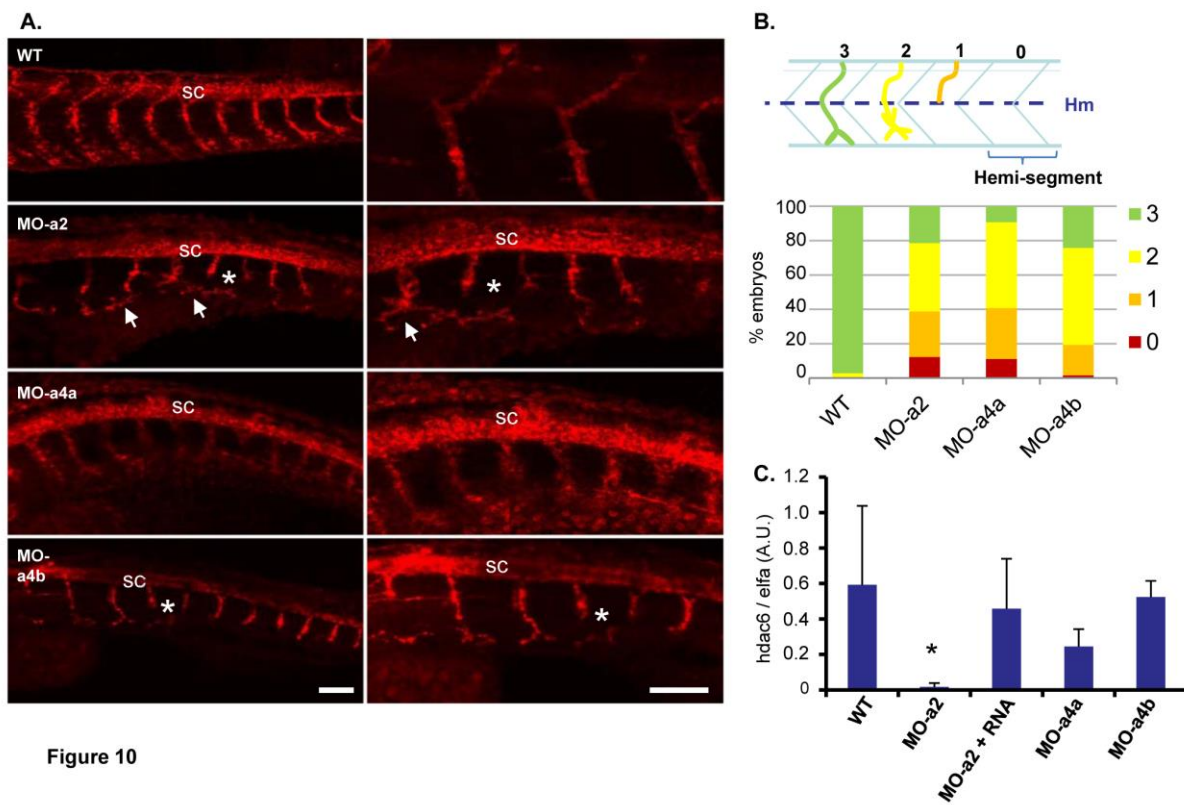


Figure 10